New Journal of Physics
The open-access journal for physics

Cold injection for electron wakefield acceleration

X Davoine[1], A Beck[1], A Lifschitz[3], V Malka[2] and E Lefebvre[1,4]

[1] CEA, DAM, DIF, 91297 Arpajon, France
[2] Laboratoire d'Optique Appliquée, ENSTA, CNRS, Ecole Polytechnique, UMR 7639, 91761 Palaiseau, France
[3] Laboratoire de Physique des Gaz et Plasmas, CNRS UMR 8578, Université Paris XI, Bâtiment 210, 91405 Orsay, France
E-mail: erik.lefebvre@cea.fr

New Journal of Physics **12** (2010) 095010 (23pp)
Received 12 February 2010
Published 24 September 2010
Online at http://www.njp.org/
doi:10.1088/1367-2630/12/9/095010

Abstract. The present paper elaborates on the cold injection scheme, which was recently proposed in the context of laser wakefield acceleration (Davoine *et al* 2009 *Phys. Rev. Lett.* **102** 065001). This scheme allows one to inject a bunch of electrons into a laser wakefield, which is possible thanks to the collision between the main and a counter-propagating laser pulse. Unlike in the conventional colliding pulse schemes, in this process, a beatwave is created during the collision, which allows the injection of electrons with negligible heating. In this paper, we show that the injection of on-axis electrons observed in simulations is well described by a one-dimensional (1D) model, as long as conditions given here are satisfied. Injection of off-axis electrons is also influenced by transverse effects, but the basic mechanisms remain the same. Then, a comparison with the conventional colliding pulse schemes shows that each scheme can occur in different regimes. In particular, cold injection proves to be more interesting regarding the energy spread issue. Indeed, the simulations demonstrate that electron bunches with sub-MeV absolute energy spreads can be injected, leading, after acceleration, to electrons at several GeV and relative energy spread below 1%.

[4] Author to whom any correspondence should be addressed.

Contents

1. Introduction

Over the last few years, remarkable advances in the laser-wakefield acceleration of electrons [1] have been achieved. In particular, since the production of the first experimental quasi-monoenergetic spectra [2]–[4], GeV energy has been achieved [5, 6] after acceleration in plasmas a few centimetres long. In parallel, guided propagation [7] and acceleration [5] in a capillary have been demonstrated, and the use of optical injection has proved that it is possible to stabilize and control electron beams [8]–[11]. More recently, controlling the electron beam parameters with an optical injection scheme has made it possible to produce beams with relative energy spread as small as 1% [12]. This new result is relevant to high-quality and short x-ray pulse production [13]. However, in the Free Electron Laser concept, utilizing an electron beam with an even lower energy spread, is required for producing x-rays [14]. Therefore, to use laser-wakefield technology in future systems, further improvements of the beam quality are required. Optical injection schemes seem to be one of the best-suited approaches to enhance both the quality and the control of electron beams.

To be accelerated to high energy, electrons must first be trapped in the propagating wakefield. These electrons can then reach the wake velocity and be accelerated to high energy. If the wakefield amplitude is large enough, some background plasma electrons can be accelerated up to the wake velocity, in a process known as self-injection. Alternatively, injection can be triggered by a plasma density gradient [15] or by tunnel-ionization [16, 17], which are two potential approaches to control the electron injection and, as a consequence, the characteristics of the final beam. In optical injection schemes, additional laser pulses are used to cause electron injection and several arrangements have been proposed over recent years.

Optical injection was first proposed in [18]. In this initial implementation, the injection is triggered by a second laser pulse (injection pulse) coming perpendicularly to the pulse generating the wakefield (pump pulse). When the injection pulse collides with the wakefield, the transverse ponderomotive force of the pulse provides some electrons with the necessary momentum to be trapped in the wake. The same scheme was used in [19], but the authors show that wake–wake collision can also give to some electrons the necessary momentum for injection and trapping. A third scheme [20] uses three laser pulses instead of two and operates in a collinear geometry. A pump pulse creates the wakefield, while two other counter-propagating

pulses collide inside the wake. Electrons are heated in the collision and, as in the first case, those with enough momentum are trapped. This scheme has then been simplified [21, 22] by keeping the collinear geometry but using only two pulses. The pump pulse still creates the wakefield but also collides with the second pulse coming from the opposite direction. This collision, as before, heats the electrons and some of them can then be trapped. This later scheme, known as the colliding pulse scheme, has been used in the first successful experimental demonstration of optical injection [8].

In the cold injection scheme that we recently proposed in [23], electrons are also optically injected, but the injection relies on a mechanism fundamentally different from previous schemes, since no momentum gain is needed. Therefore, the cold injection scheme can benefit from the same advantages as the previous colliding pulse scheme—such as the possibility to tune the electron beam energy by modifying the position of the injection inside the plasma [8]. Also, it has additional advantages. As we will see later, there are some laser and plasma parameter ranges for which cold injection is possible, whereas conventional colliding pulse injection cannot occur. In addition, a bunch of electrons can be injected with low initial momentum and energy spreads, as no heating is needed. The first studies that we carried out confirm that this scheme is a promising method to generate electron beams with very low energy spread and good quality [23]. In the present paper, we investigate this scheme in more detail to show its advantages and its limitations.

The structure of this paper is as follows. In section 2, the principle of the cold injection scheme is described theoretically in a one-dimensional (1D) geometry. Then a first example coming from a 2D simulation is given in section 3, highlighting the injection mechanisms in a more realistic case. We will see in section 4 that this cold injection can occur only when specific conditions are fulfilled. In section 5, the transverse effects are discussed: the 1D cold injection description is extended to a multidimensional case. A comparison between the colliding pulse scheme and the cold injection scheme is made in section 6. Then, in section 7, the injection and acceleration of high-quality beams using this scheme are discussed. The conclusions are given in section 8.

2. Principle

To introduce the cold injection principle, we present a 1D analysis that gives a qualitative understanding of the physics involved. In this paper, unless units are explicitly given, time and space coordinates are normalized to, respectively, ω_0^{-1} (the laser pulsation) and k_0^{-1} (wavenumber), and the mass and charge are normalized to, respectively, m_e (the electron mass) and e (its charge). Other quantities are also given in normalized units. In the following, the laser wavelength is $\lambda_0 = 0.8\,\mu$m. Subscript 0 and 1 always denote the main pulse creating the wake and the injection pulse, respectively.

Before providing a description of the injection mechanisms, we first recall some results on wakefield acceleration. Assuming that all of the fields are quasi-static, they only depend on the wake phase $\zeta = x - \beta_p t$, where β_p is the laser pulse velocity, which is equal to the wake phase velocity. The motion of electrons in the wakefield is then described by the following Hamiltonian [24],

$$H(\zeta, p_x) = \sqrt{\gamma_\perp^2(\zeta) + p_x^2(\zeta)} - \beta_p p_x - \Psi(\zeta), \tag{1}$$

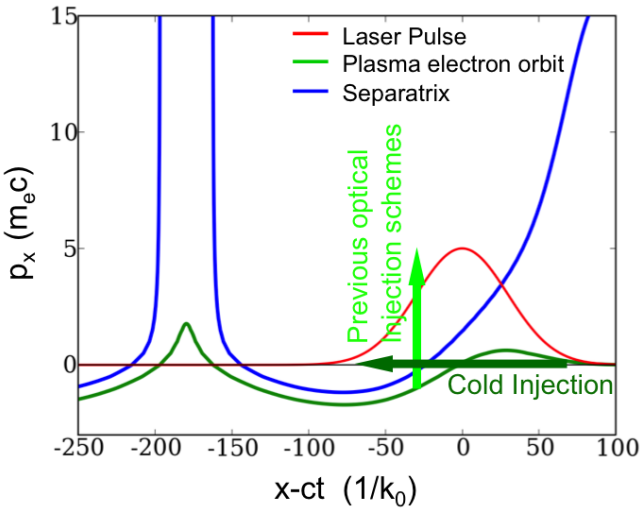

Figure 1. Cold injection principle: electrons are injected by being dephased from the front of the main pulse to its back without momentum gain (dark green arrow). After dephasing, electrons are effectively injected over the separatrix. Dephasing is achieved by the collision with a counter-propagating laser pulse. In comparison, in previous optical injection schemes, injection is achieved thanks to momentum gain (light green arrow).

where $\gamma_\perp = (1+\mathbf{p}_\perp{}^2)^{1/2}$, $\mathbf{p}_\perp$ and p_x are the electron transverse and longitudinal momenta, and $\Psi(\zeta) = \Phi(\zeta) - \beta_\mathrm{p} A_x(\zeta)$ with Φ and A_x, respectively, being the scalar potential and longitudinal vector potential. As this Hamiltonian is not time dependent, an electron with a phase ζ_0 and a longitudinal momentum p_{x0} is characterized by its Hamiltonian $H_0 = H(\zeta_0, p_{x0})$ and the evolution of its longitudinal momentum can be written as

$$p_x(\zeta) = \beta_\mathrm{p}\gamma_\mathrm{p}^2(H_0 + \Psi(\zeta)) \pm \gamma_\mathrm{p}\sqrt{\gamma_\mathrm{p}^2(H_0 + \Psi(\zeta))^2 - \gamma_\perp^2(\zeta)}, \tag{2}$$

where $\gamma_\mathrm{p} = (1-\beta_\mathrm{p}^2)^{-1/2}$. From this equation, two kinds of orbits can be observed in phase space. For a high enough value of H_0, the term $(\gamma_\mathrm{p}^2(H_0+\Psi(\zeta))^2 - \gamma_\perp^2(\zeta))^{1/2}$ is well defined for all ζ. This case corresponds to untrapped electrons: they slip backward with time in the wakefield. For lower values of H_0, orbits of electrons in the phase space are closed: this case corresponds to electrons that are trapped in a wakefield bucket. Those electrons can be accelerated to high energy. The boundary between trapped and untrapped orbits (the separatrix) is given by a critical value, H_c, of the Hamiltonian. The separatrix equation is thus

$$p_{x\mathrm{c}}^{\pm}(\zeta) = \beta_\mathrm{p}\gamma_\mathrm{p}^2(H_\mathrm{c} + \Psi(\zeta)) \pm \gamma_\mathrm{p}\sqrt{\gamma_\mathrm{p}^2(H_\mathrm{c} + \Psi(\zeta))^2 - \gamma_\perp^2(\zeta)}. \tag{3}$$

Before interacting with the laser pulse, plasma electrons are at rest with $\Psi = 0$. These electrons follow the same orbit characterized by $H_\mathrm{p} = H(p_x = 0, \Psi = 0) = 1$,

$$p_{x\mathrm{p}}(\zeta) = \beta_\mathrm{p}\gamma_\mathrm{p}^2(1 + \Psi(\zeta)) - \gamma_\mathrm{p}\sqrt{\gamma_\mathrm{p}^2(1 + \Psi(\zeta))^2 - \gamma_\perp^2(\zeta)}. \tag{4}$$

When the self-injection threshold is not reached, the $p_{x\mathrm{p}}(\zeta)$ orbit is under the separatrix $p_{x\mathrm{c}}^{-}(\zeta)$, as shown in figure 1. In optical injection schemes, an injection laser pulse is used to move electrons from the background plasma up to the trapped orbits in order to inject them.

With previous schemes, the injection pulse is used to provide some electrons with the necessary momentum to cross the separatrix.

In the cold injection scheme, the injection is achieved by dephasing some electrons during the pulse collision so that they slip backward in the wake and be trapped in the first wakefield bucket at the back of the laser pulse. A collision with a low energy and counter-propagating laser pulse is used to cause this electron dephasing. Indeed, when two circularly polarized pulses collide, a beatwave force is created [20, 23, 25], which is spatially periodic with a $\lambda_0/2$ wavelength. Under certain conditions that we will derive below, this beatwave force can dominate the longitudinal ponderomotive force of the main pulse. Electrons are then trapped inside the small-scale beatwave buckets and cannot have the large longitudinal motion normally caused by the ponderomotive force alone. As their longitudinal motion is frozen by the beatwave, electrons are blocked as the wake goes by, effectively slipping backward in the wake frame of reference. After the collision, they finally enter the wake bucket with negligible longitudinal momentum, as shown in figure 1.

To understand cold injection more precisely, we need to investigate the competition between the ponderomotive and beatwave forces more realistically. To this end, let us consider the collision between two circularly polarized pulses with Gaussian temporal profiles. For the sake of simplicity, we still consider a 1D geometry. The motion of an electron in vacuum and under the influence of the two counter-propagating pulses is first analyzed. We will then develop a simple analytic model that can predict which electrons will be dephased, and the amplitude of their phase shifts.

First, we consider the motion of an electron when the normalized vector potentials of the two pulses read

$$\mathbf{A_0}(x,t) = \tilde{A}_0(x,t)[\cos(t-x)\mathbf{e_y} + \sin(t-x)\mathbf{e_z}], \tag{5}$$

$$\mathbf{A_1}(x,t) = \tilde{A}_1(x,t)[\cos(t+x)\mathbf{e_y} + \sin(t+x)\mathbf{e_z}] \tag{6}$$

with envelopes given by

$$\tilde{A}_0(x,t) = \frac{a_0}{\sqrt{2}}\,\mathrm{e}^{-2\ln(2)(t-x/\tau_0)^2}, \tag{7}$$

$$\tilde{A}_1(x,t) = \frac{a_1}{\sqrt{2}}\,\mathrm{e}^{-2\ln(2)(t+x/\tau_1)^2}, \tag{8}$$

where a_0 and a_1 are the normalized vector potentials of the main and injection pulses. According to this definition, the full overlap of the two pulses occurs when $t = x = 0$.

The motion of an electron in those fields is characterized by the following Hamiltonian,

$$H(p_x,x,t) = \gamma = \sqrt{1 + (\mathbf{A_0}(x,t) + \mathbf{A_1}(x,t))^2 + p_x^2}, \tag{9}$$

where γ is the electron Lorentz factor. The electron equation of motion is then given by

$$\frac{\mathrm{d}p_x}{\mathrm{d}t} = -\frac{\partial H}{\partial x} = -\frac{1}{2\gamma}\frac{\partial \tilde{A}_0^2}{\partial x} - \frac{1}{2\gamma}\frac{\partial \tilde{A}_1^2}{\partial x} - \frac{1}{2\gamma}\frac{\partial}{\partial x}(2\tilde{A}_0\tilde{A}_1\cos(2x)). \tag{10}$$

To determine if an electron will be dephased, we now discuss the influence of each of the three terms in the right-hand side of equation (10). We first focus on the third term. This corresponds to the beatwave force F_b, which can be expressed as

$$F_\mathrm{b} = -\frac{1}{\gamma}\frac{\partial \tilde{A}_0}{\partial x}\tilde{A}_1\cos(2x) - \frac{1}{\gamma}\frac{\partial \tilde{A}_1}{\partial x}\tilde{A}_0\cos(2x) + \frac{2}{\gamma}\tilde{A}_0\tilde{A}_1\sin(2x). \tag{11}$$

We consider that the pulse durations are long enough so that $\tau_0 \gg 1$ and $\tau_1 \gg 1$. In that case, $\partial \tilde{A}_0/\partial x \sim a_0/\tau_0 \ll a_0$ and $\partial \tilde{A}_1/\partial x \sim a_1/\tau_1 \ll a_1$ so that the first two terms of the force F_b can be neglected in front of the third term. Thus, we are left with

$$F_\mathrm{b} \approx \frac{2}{\gamma}\tilde{A}_0\tilde{A}_1 \sin(2x). \tag{12}$$

This expression for the beatwave force is similar to that given in [20, 23, 25], where two infinite pulses are considered ($\tilde{A}_0 = a_0/2^{1/2}$ and $\tilde{A}_1 = a_1/2^{1/2}$). The use of circular polarizations for the two pulses is required to get this specific beatwave force. For example, as explained in [25], some additional terms appear in this force if linear and parallel polarizations are used, which can cause a strong heating of the plasma and prevent the trapping of the electrons inside the beatwave buckets.

The first and second terms in the right-hand side of equation (10) correspond to the ponderomotive force of the two pulses. As the injection pulse amplitude is low, its ponderomotive force can be neglected in front of the ponderomotive force of the main pulse. The first term can be expressed as

$$F_\mathrm{p} = -\frac{1}{2\gamma}\frac{\partial \tilde{A}_0^2}{\partial x} = \frac{4\ln(2)}{\gamma\tau_0^2}(x-t)\tilde{A}_0^2. \tag{13}$$

Therefore, an electron can be trapped in the beatwave buckets and dephased with respect to the wakefield only if the beatwave force is the prevailing component of the total force. Thus, the electron is dephased only if the following condition is satisfied,

$$\chi \equiv \frac{F_\mathrm{b}/\sin(2x)}{|F_\mathrm{p}|} = \frac{\tau_0^2\tilde{A}_1}{2\ln(2)\,|x-t|\,\tilde{A}_0} > 1, \tag{14}$$

where $|F_\mathrm{p}|$ is the absolute value of F_p. F_b is divided by $\sin(2x)$ to keep only the envelope of the beatwave force. The boundary where $\chi = 1$ is defined by the following two equations,

$$x = -t - \Delta(\xi), \tag{15}$$

$$x = -t + \Delta(\xi), \tag{16}$$

where $\xi = t - x$ is the phase relative to the main pulse, and Δ is defined as

$$\Delta(\xi) = \sqrt{\frac{\tau_1^2}{\tau_0^2}\xi^2 - \frac{\tau_1^2}{2\ln 2}\ln\left(\frac{2\ln(2)a_0}{\tau_0^2 a_1}\,|\xi|\right)}. \tag{17}$$

This boundary and both regions are represented in figure 2 for a given set of parameters. Electrons can be dephased where the beatwave force is dominating, which corresponds to the red region.

A second condition for dephasing should also be considered, as it is only relevant to consider the competition between the beatwave and ponderomotive forces where the main pulse intensity is significant. Outside this region, both forces are negligible and injection cannot occur. We thus introduce a limit value a_L for the normalized vector potential and only consider what happens where $\tilde{A}_0 > a_\mathrm{L}$. This condition corresponds to the region where

$$|t-x| < \frac{\tau_0}{\sqrt{2\ln(2)}}\sqrt{\ln\left(\frac{a_0}{\sqrt{2}a_\mathrm{L}}\right)} \equiv \xi_L. \tag{18}$$

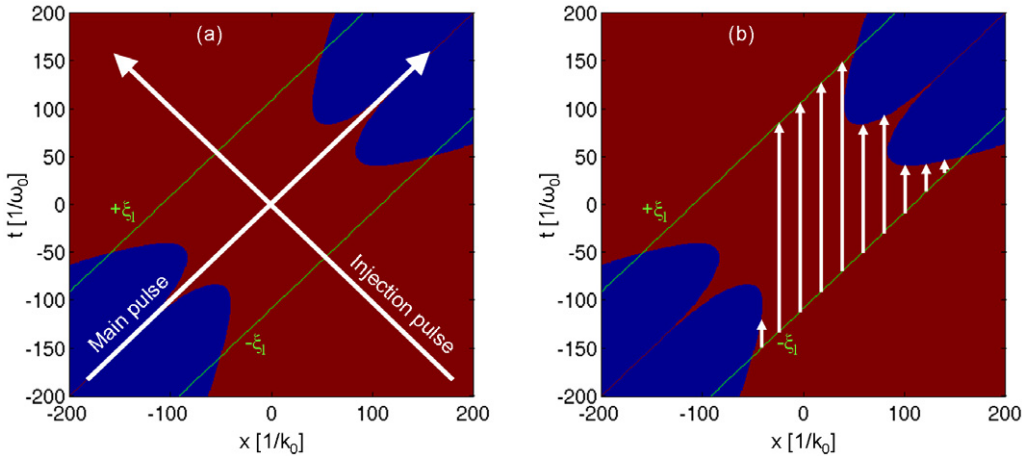

Figure 2. Scheme of beatwave dephasing in 1D. The red and blue regions correspond, respectively, to $\chi(x,t) > 1$ and $\chi(x,t) < 1$ when $a_0 = 4$, $\tau_0 = 30$ fs, $a_1 = 0.1$ and $\tau_1 = 60$ fs. (a) Trajectories of the main pulse and injection pulse are represented. (b) Simplistic trajectories of electrons when they interact with the main pulse and when the beatwave force is dominating are represented by white arrows.

In the space–time plot represented in figure 2, this region is delimited by the two green lines labeled by $-\xi_L$ (main pulse front) and $+\xi_L$ (main pulse back). The value $a_L = 0.1$ has been used in this figure.

A third and last condition should be considered to determine the dephasing. Electrons passing through the region where the ponderomotive force is stronger ($\chi < 1$) while they interact with the main pulse ($-\xi_L < \xi < \xi_L$) are no longer considered as being dephased. Thus, even if they enter afterwards in the region where the beatwave is stronger ($\chi > 1$), they cannot be trapped in the beatwave and be dephased. This is due to the fact that they can gain enough momentum when they are first accelerated by the ponderomotive force to then pass from bucket to bucket and not be trapped by the beatwave.

With those three conditions, we can now determine the simplistic trajectories of dephased electrons. A few examples are shown in figure 2(b). Those electrons are dephased from the front of the main pulse to either the back of the main pulse or the region where $\chi < 1$. During its dephasing, the longitudinal position of an electron does not evolve on a distance larger than $\lambda_0/2$ (as the dephased electron is trapped in the beatwave buckets), which gives quasi-vertical trajectories in figure 2(b).

3. Example of cold injection

In this section, we present the results of a simulation modeling a more realistic case: we have considered a 2D geometry and the fields generated by the plasma are no longer neglected. We present these results with two objectives: first we validate the theoretical description of dephasing made in the previous section and then we give an example showing the full cold injection process, with dephasing and injection.

In this simulation, the two colliding pulses are characterized by $a_0 = 4$, $\tau_0 = 30$ fs, and $a_1 = 0.2$, $\tau_1 = 60$ fs. The focal spot sizes (full width at half maximum (FWHM) of the intensity)

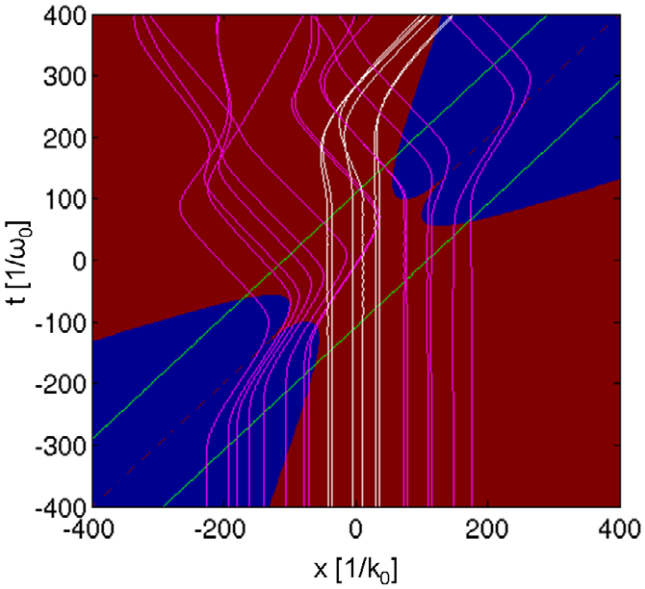

Figure 3. Trajectories of randomly chosen electrons coming from a 2D simulation. $a_0 = 4$, $\tau_0 = 30$ fs, $\Phi_0 = 18\,\mu$m and $a_1 = 0.2$, $\tau_1 = 60$ fs, $\Phi_1 = 5\,\mu$m. Trajectories of injected (non-injected) electrons are plotted in white (pink). The $\chi > 1$ ($\chi < 1$) region is shown in red (blue).

are $\Phi_0 = 18\,\mu$m and $\Phi_1 = 5\,\mu$m, respectively. We have chosen a small value for Φ_1 so that only the electrons near the propagation axis are dephased. Transverse effects are reduced, since the transverse wakefields and the transverse ponderomotive force are negligible on the axis. Therefore, even in this 2D simulation, we keep a '1D-like' dephasing mechanism. The plasma density is $n_{e0} = 2.5 \times 10^{-4} n_c$, where $n_c = m_e \epsilon_0 \omega_0^2 / e^2$ is the critical density and ϵ_0 the permittivity of free space. In addition, the density is parabolic in the transverse direction: $n_e(r) = (1 + r^2/R^2) n_{e0}$, where r is the radial position and $R = 27\,\mu$m is a value chosen to provide good guiding of the main pulse. We have run simulations with the PIC code CALDER [26], in which the ions have been treated as a fixed background. We have checked that no electron is injected when the second laser is turned off, whereas an electron bunch is injected if the laser pulse collision occurs.

To validate the theoretical description of dephasing made in the previous section, we have randomly chosen particles close to the propagation axis and tracked their longitudinal position with time. These trajectories are plotted in figure 3. The region where $\chi > 1$ and $\chi < 1$ is also represented. The electrons that are finally injected are in white, and the other electrons are in pink. Before the interaction with the main pulse, electrons remain static and follow vertical trajectories in figure 3. During their interaction with the main pulse, either the electrons are in a blue region and are pushed forward or backward by the ponderomotive force, or they are in the red region and they keep a vertical trajectory, as they are trapped in the beatwave before being accelerated by the wakefield. The clear difference in behavior between red and blue regions is a good validation of the theoretical determination of dephasing developed in the previous section.

We can also observe in figure 3 that only electrons that keep a vertical trajectory when they are overtaken by the back of the main pulse are injected. Those vertical trajectories mean that injected electrons have almost zero longitudinal velocity, showing that this dephasing

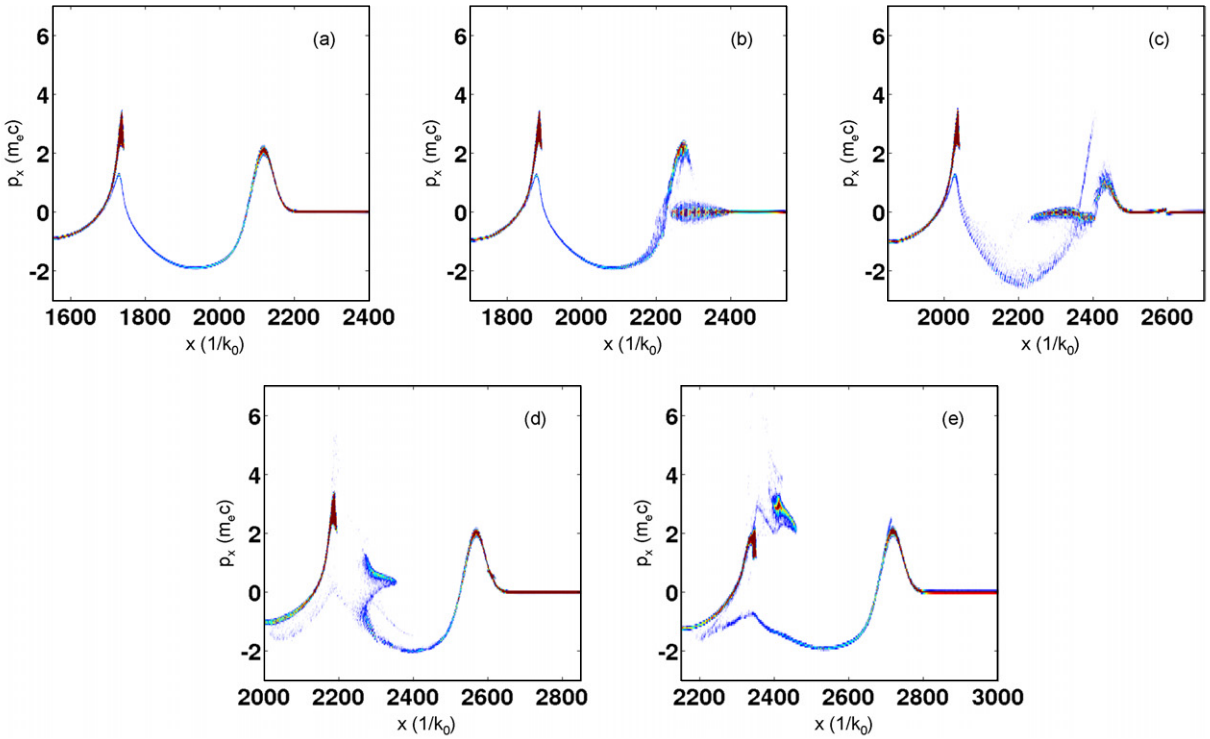

Figure 4. Phase-space plots of plasma electrons taken at five different times during the injection process. Only electrons located near the propagation axis are plotted. 2D simulation, $a_0 = 4$, $\tau_0 = 30$ fs, $\Phi_0 = 18\,\mu$m and $a_1 = 0.2$, $\tau_1 = 60$ fs, $\Phi_1 = 5\,\mu$m.

occurs without energy gain. Other electrons, which have been accelerated by the main pulse ponderomotive force and by the wakefield, have a negative longitudinal velocity when they are overtaken by the back of the main pulse and oscillate afterwards in the wake without being injected.

To confirm that dephased electrons retain a low longitudinal velocity and stay 'cold' during the pulse collision, we present in figure 4 five snapshots of the plasma phase space. This figure also confirms that it is the dephased electrons that are injected into the wake. Only electrons near the propagation axis are plotted. Before collision, in figure 4(a), electrons oscillate in the wake as usual. When collision starts, we can see in figure 4(b) that electrons trapped in the beatwave (electrons located between $x = 2200k_0^{-1}$ and $x = 2400k_0^{-1}$) are no longer accelerated forward by the main pulse ponderomotive force: they oscillate in the beatwave buckets with low longitudinal momentum. They still have this low momentum at the end of the pulse collision, in figure 4(c). Consistently, they are still located at the same position, between $x = 2200k_0^{-1}$ and $x = 2400k_0^{-1}$, while the main pulse and the wake have propagated. Those electrons have thus effectively been dephased with very low momentum gain. After collision, figures 4(d) and (e) show that the dephased electron bunch is then accelerated by the wakefield. Those electrons are trapped in the wake and can later be accelerated to high energy.

During the collision, we can see in figures 4(b) and (c) that dephased electrons get a small longitudinal momentum in the beatwave, leading to a low velocity spread. In order to confirm that electrons are not strongly heated by the beatwave even if the beatwave force is

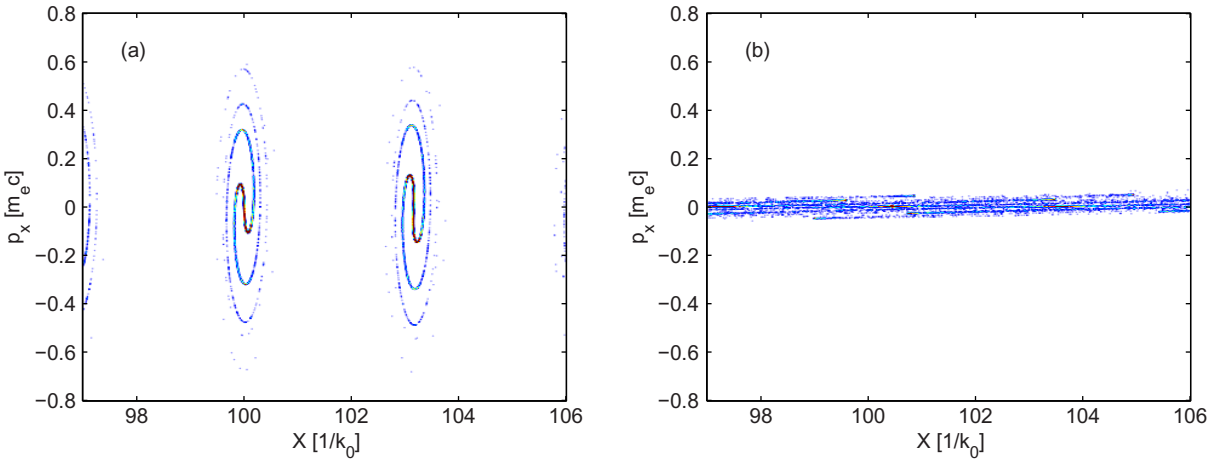

Figure 5. Electron distribution in phase space during (a) and after (b) the collision between two laser pulses. 1D simulation, $a_0 = 4$, $\tau_0 = 30$ fs, $a_1 = 0.2$, $\tau_1 = 45$ fs and $n_e = 10^{-8} n_c$.

strong, we have performed an additional simulation in which we only consider the electrons evolution in the beatwave. For the sake of simplicity, this simulation has been run in 1D and we have used a very low value for plasma density ($n_e = 10^{-8} n_c$), so plasma effects are negligible. Figure 5 shows the electron distribution in phase space during and after the pulses collision in this simulation. We can observe in figure 5(a) that the electrons oscillate in the beatwave buckets. The $\lambda_0/2$ periodicity, corresponding to the beatwave wavelength, is well observed. After the collision, in figure 5(b), electrons can propagate freely. We can see that they have gained some longitudinal momentum due to the collision, providing a momentum spread to the plasma. However, this spread is lower than $\Delta p_x = 0.1 m_e c$. This result is consistent with the more realistic case presented in figure 4(c) and confirms that electron heating during the dephasing is kept at a low level, leading to a 'cold' dephasing and injection of electrons into the wake. A comparison with the previous colliding pulse scheme in which a strong heating occurs and is even necessary for injection is presented in section 6.

4. Conditions of existence

We review in this section the conditions that should be fulfilled for cold injection to take place. First of all, to create a beatwave and avoid strong stochastic heating [27]–[29], circular polarizations should be used [25], as presented in equation (6). Then, to be injected, electrons should be able to cross the separatrix despite their small longitudinal momentum. The second condition is therefore that the wakefield amplitude should be large enough for the separatrix to cross the $p_x = 0$ axis, as illustrated in figure 2. If we denote by 'cold trapping region' the region where the separatrix is under the $p_x = 0$ axis, then electrons should be dephased up to this area to be injected. A scheme of the cold trapping region is given in figure 6.

In addition to being defined as the region where the separatrix is under the $p_x = 0$ axis, the cold trapping region can also be determined with a condition on the wake potential Ψ. This second definition can be easier to use as there is no need to calculate the separatrix. To obtain this condition on Ψ, we assume that an electron is trapped if it is accelerated to the wake velocity

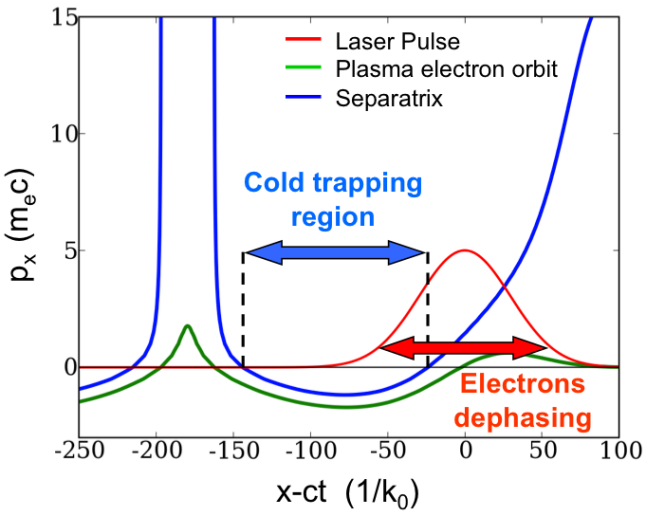

Figure 6. Scheme of the cold trapping region and of the region where electrons can be dephased.

before reaching the back of the accelerating region. It therefore reaches this velocity in a region where Ψ satisfies $\Psi > \Psi_c$, where Ψ_c is the wakefield potential at the back of the accelerating region. Its Hamiltonian then satisfies $H < H_c$ with

$$H_c = \gamma - \beta_p p_x - \Psi_c = \frac{\gamma_\perp}{\gamma_p} - \Psi_c, \tag{19}$$

where p_x, γ and $\gamma_\perp$ are the characteristics obtained by the electron when it reaches the wake velocity, which means that we have $p_x = \gamma\beta_p$. As we can consider that dephased electrons enter the wake with a negligible momentum, the 1D Hamiltonian of an electron injected at position ζ is simply

$$H = 1 - \Psi(\zeta). \tag{20}$$

Thus, the condition $H < H_c$ leads to

$$\Psi(\zeta) > 1 - \frac{\gamma_\perp}{\gamma_p} + \Psi_c. \tag{21}$$

Assuming that $\gamma_p \gg 1$ and $\gamma_\perp \sim 1$, we then have $\Psi(\zeta) \gtrsim 1 + \Psi_c$. Thus, the region where this condition is satisfied corresponds to the cold trapping region. Such a region exists if $\Psi_{max} - \Psi_c \gtrsim 1$, which sets a condition on the wake amplitude. According to [17], this condition $\Psi_{max} - \Psi_c \gtrsim 1$ is reached in the matched blowout regime where $a_0 \gtrsim 2$.

As dephasing can only occur up to the back of the main pulse, where $\xi = \xi_L$, the cold trapping region should be large enough and extend up to the back of the laser pulse, as shown in figure 6. This emphasizes the need to generate a large wake, indicating that cold injection is not suited to the linear regime of wakefield generation, with a low value for a_0.

A last condition should be fulfilled for the occurrence of cold injection. As the beatwave perturbs the electron motion, the wake is not well generated in the collision region. This mechanism, known as wake inhibition [30], can strongly affect the wakefield in the collision region. Yet for a successful cold injection, electrons must be accelerated by the wakefield right after being dephased, so they can gain momentum and be injected. Thus, if the wakefield is inhibited too much, this will preclude acceleration and injection of the dephased electrons. Therefore, wake inhibition should be kept at a low level to allow the cold injection.

For example, the magnitude of wake inhibition is illustrated in figure 7 in the case of the 2D simulation already presented in figure 4. This figure displays the evolution of the plasma wake and on-axis wakefield during pulse collision and electron injection. The electric field profile in figure 7(f) is also plotted as a dotted blue line in figures 7(g)–(j), so the fields after collision can be compared with the initial profile. We can see that the wakefield is perturbed by the collision, but this modification is relatively small, so that dephased electrons can still be accelerated by the wakefield and be injected.

The wakefield in the first bubble is created by all the electrons forming the bubble. If a small fraction of those electrons are perturbed by the collision, then the wakefield will only be slightly inhibited. The number of electrons forming the bubble is roughly proportional to the volume of the bubble. The number of perturbed electrons, on the other hand, is roughly proportional to the volume of the collision region. Therefore, the last condition for the existence of cold injection is that the volume of the collision region should be much smaller than the volume of the bubble.

The collision region length and width are respectively $c(\tau_0 + \tau_1)/2$ and $\min(\Phi_0, \Phi_1)$. In the 2D simulation presented in figure 7, an estimate of the 2D bubble volume is $500 \times 300 k_0^{-2}$. In comparison, the collision region volume is $105 \times 40 k_0^{-2}$. Thus, the collision volume is much smaller than the bubble volume, explaining why the wake inhibition is small in figure 7. In this simulation, thanks to the use of a low plasma density, the plasma wavelength is much larger than the pulse length, leading to a bubble volume much larger than the collision region volume.

In the first successful experiment using the colliding pulse scheme [8], a beatwave was generated during the collision and some electrons may have been dephased, but the bubble volume and the collision region volume were of the same order of magnitude. As a result, a strong wake inhibition occurred [25] and prevented cold injection from playing a role. Therefore, in this experiment, only electrons heated during the collision were injected. Heating was achieved by a combination of beatwave heating and stochastic heating, both provided by the collision between two pulses with linear and parallel polarizations.

5. Transverse effects

When an injection pulse with a large waist is used, off-axis electrons can also be injected. In this case, transverse effects should be taken into account. These transverse effects slightly modify both electron dephasing during the collision and electron injection.

We first start with a description of electron injection. The cold trapping region should now be determined in 3D geometry. Assuming radial symmetry, the Hamiltonian given in equation (1) becomes

$$H(\zeta, r, p_x, p_\perp) = \sqrt{1 + p_\perp^2 + p_x^2} - \beta_\mathrm{p} p_x - \Psi(\zeta, r), \tag{22}$$

where r is the radial position. The cold trapping region is then defined by

$$\Psi(\zeta, r) > 1 - \frac{\gamma_\perp}{\gamma_\mathrm{p}} + \Psi_\mathrm{c}, \tag{23}$$

where Ψ_c is now the potential at the back of the accelerating and focusing region. As before, we can neglect the $-\frac{\gamma_\perp}{\gamma_\mathrm{p}}$ term to derive approximate expressions for the existence and size of the cold trapping region. However, in a multidimensional geometry, off-axis electrons can gain a significant transverse momentum during their injection. For those electrons, the $-\frac{\gamma_\perp}{\gamma_\mathrm{p}}$ term

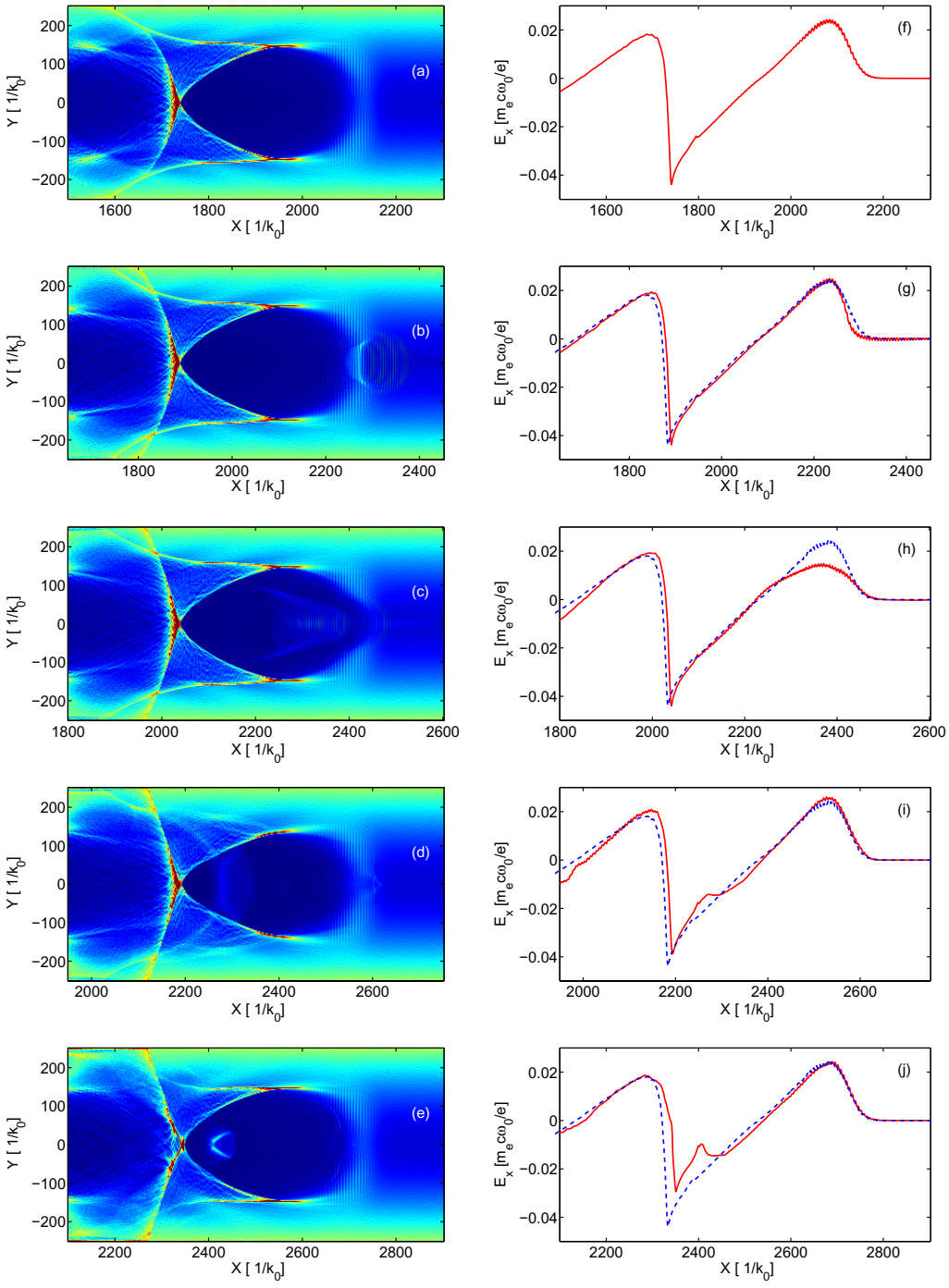

Figure 7. Evolution of the electron density (a, b, c, d, e) and of the on-axis longitudinal electric field (f, g, h, i, j) while collision and injection occur. Electric field is plotted in red, and the initial electric field (f) is repeated in the following figure with a dotted blue line. 2D simulation, $a_0 = 4$, $\tau_0 = 30\,\mathrm{fs}$, $\Phi_0 = 18\,\mu\mathrm{m}$ and $a_1 = 0.2$, $\tau_1 = 60\,\mathrm{fs}$, $\Phi_1 = 5\,\mu\mathrm{m}$. The initial transverse electron density is parabolic.

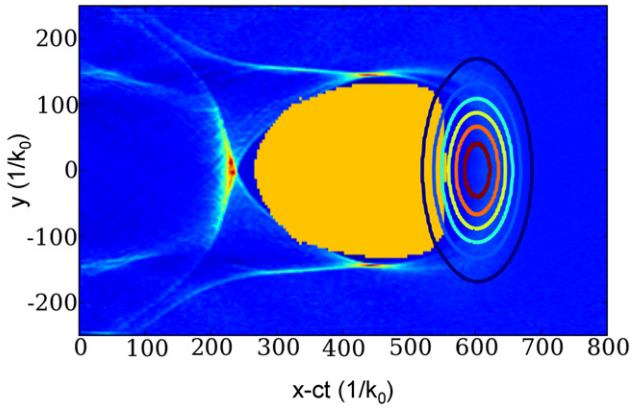

Figure 8. The cold-trapping region (shown in yellow) in a 2D example. The electron density map is shown in the background. Iso-values of the pulse intensity are shown by colored ellipses. The wake used in this figure is the wake calculated in the simulation presented in section 3.

cannot be neglected. To take this into account, we need to know the value of $\gamma_\perp$ at the end of the injection, when the particle reaches the wake velocity, and this can be done by calculating the particle trajectory. Therefore, to fully determine the cold trapping region, we need to follow trajectories of particles inserted at rest at different locations in the wakefield bucket and check if they are finally trapped.

This has been calculated for the case of the quasi-static wake presented in section 3, and the result is plotted in figure 8. All electrons inserted at rest in the yellow region are found to eventually reach the wake velocity and be injected. We can see that, in this case, the cold trapping region is quite large and extends to the back of the laser pulse. This confirms that cold injection can occur in that case, even for off-axis electrons.

In the blowout regime [31], without collision, the off-axis electrons are pushed sideways by the transverse ponderomotive force and by the fields created by the plasma. Most of these electrons propagate in a narrow sheath forming the boundary of the bubble. However, as can be seen in figure 8, this boundary is located further from the axis than the limit of the cold trapping region. A detailed study of the trajectory of an injected electron coming from an off-axis position is described in [23]. This study has shown two results: (i) even if this electron is at an off-axis position where the intensities of the two laser pulses are low, this electron is well trapped in the beatwave and is dephased; (ii) it is also pushed sideways less than in the case without collision. This second result is important, as it shows that, thanks to the collision, off-axis electrons are not pushed sideways up to the sheath position but can stay inside the bubble and enter the cold trapping region.

In some simulations, we observe that the off-axis electrons are more easily injected than on-axis electrons. This behavior occurs when the colliding pulse is too short to dephase on-axis electrons over a long enough distance to cross the separatrix. To illustrate this, we run a 2D simulation similar to the one presented in section 3, except that the plasma density is now constant ($n_e = 2.5 \times 10^{-4} n_c$) and the injection pulse parameters are now $a_1 = 0.1$, $\tau_1 = 30$ fs and $\Phi_1 = 15\ \mu$m. In this simulation, the use of a larger spot size for the colliding pulse allows us to dephase and inject off-axis electrons. However, the short pulse duration prevents the injection

of a large number of on-axis electrons, and the majority of the electrons injected come from an off-axis position. This easier trapping of off-axis electrons is still not fully understood, but it has also been observed in the self-injection regime. For example, in the simulations presented in [32], the authors show that only electrons with an initial radial position that is lower than but close to the maximum radius of the bubble are trapped. It seems that, in our simulation, thanks to the transverse effects and to the shape of the wakefields that depend on the radial position, off-axis electrons can be injected even if the sole dephasing can hardly lead to the injection of on-axis electrons.

6. Injection due to heating versus cold injection

At first sight, the colliding pulse scheme proposed in [21, 22] and the cold injection scheme described here may seem very similar. In each scheme, a counter-propagating pulse collides with the main pulse and creates a beatwave, which can then inject electrons into the wake. The role of the beatwave, however, is different, as it is used to heat electrons in the classical colliding pulse scheme, while it is used to dephase them in the cold injection scheme.

In the previously studied cases, we have shown that heating induced by the beatwave is negligible. Therefore, with our laser and plasma conditions, the injection mechanisms described in [21, 22] do not occur. However, as explained in [25], the use of two laser pulses with linear and parallel polarizations could strongly increase electron heating during collision, as stochastic heating would also appear [27]–[29]. In this section, we therefore study the case of linear and parallel polarizations, where both cold and 'warm' injections could *a priori* co-exist. As we will see, the predominance of one or the other mechanism depends on the physical conditions.

For example, let us first consider the experiment of Faure *et al* [8]. We already mentioned at the end of section 4 that due to the laser and plasma conditions, a strong wake inhibition prevented the cold injection in this experiment and thus the warm injection was the sole mechanism leading to injection.

As a second example, we have run the same simulation as in section 3, but with linear and parallel polarizations. We have observed some heating during the collision, but this heating was too weak to lead to the injection of a significant amount of electrons. The warm injection is then negligible in comparison with the cold injection in this case. This absence of warm injection can be explained by the fact that electrons are mainly heated where the main pulse intensity is the highest. In this simulation, as the main pulse length is much shorter than the wake wavelength, this high-intensity region is located in front of the bubble (as we can see in figure 8), where the separatrix usually goes up very quickly. Thus, a strong heating is required in this case, whereas the heating found in our simulation was not sufficient and electrons were not able to cross the separatrix.

In addition to those two examples where only one of the two mechanisms leads to injection, we present here a third and last case to demonstrate that both cold and warm injections can occur at the same time. For this purpose, we have run a simulation similar to the 2D simulation presented in section 3, except that the polarizations are linear and parallel and, in order to increase stochastic heating, we have used $a_1 = 0.4$ and $\tau_1 = 45$ fs. The results are presented in figures 9(a) and (b). In addition, we have run the same simulation but with circular polarizations. In the last case, there is no stochastic heating, so the comparison of the two simulations allows us to determine the consequence of stochastic heating. The results on circular polarizations are plotted in figures 9(c) and (d).

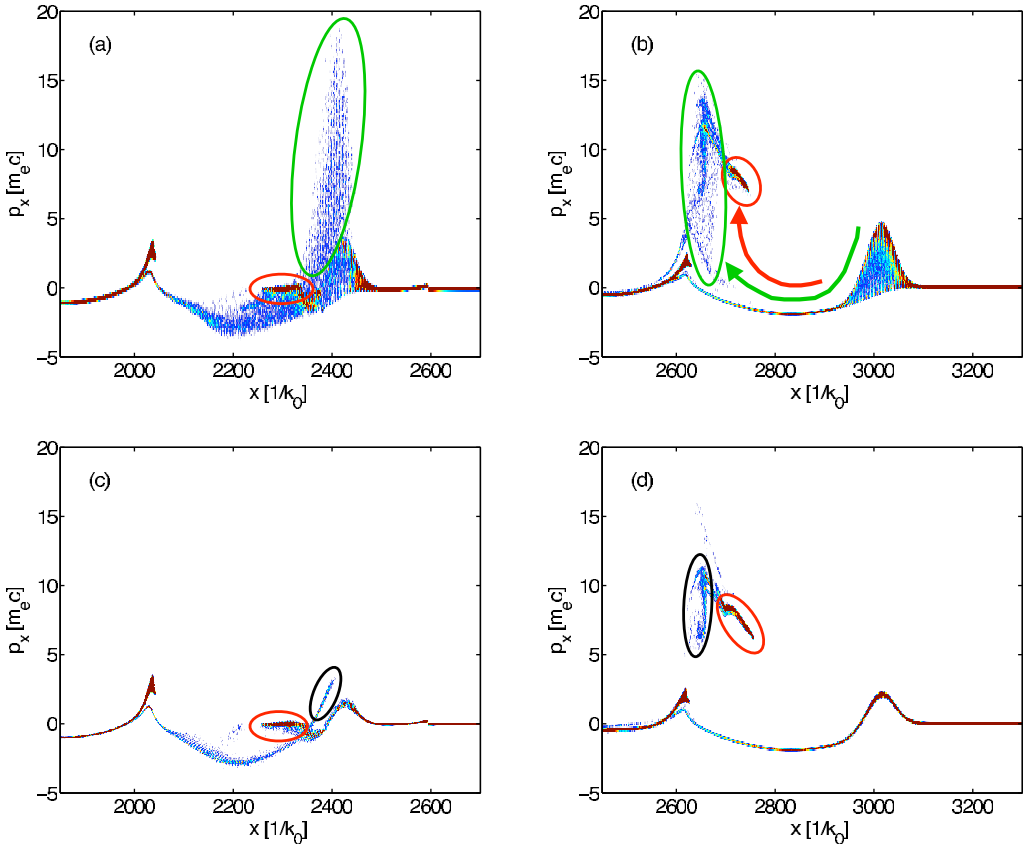

Figure 9. Phase-space plots of on-axis electrons toward the end of (a,c) and after (b,d) the pulse collision, when polarizations are linear and parallel (a,b) or circular (c,d). Red (green) ellipses show the position of the cold (warm) injected electrons. Red and green arrows show the trajectories of those groups of electrons (from figures a to b). Black ellipses show the position of a third group of electrons. The counter-propagating pulse is characterized by $a_1 = 0.4$ and $\tau_1 = 45$ fs. Red (blue) in the electron density map corresponds to a high (low) value of the density in phase space.

We have carefully followed the evolution of the electrons between the collision and their injection. As a result, in both of the polarization cases, we observe that a bunch of electrons (shown by the red ellipse in figure 9) is dephased and 'cold-injected' in the wake. In addition, in the linear polarization case, the plasma is strongly heated during the collision and the most energetic electrons can then be injected (electrons inside the green ellipse). With circular polarizations, we also observe that some electrons (in the black ellipse) are injected, even though they have been neither dephased by the beatwave nor heated. We assume that this additional injection is caused by the wake inhibition. Indeed, the wake inhibition damps down the longitudinal electric field, which is positive in front of the bubble, so the wakefield becomes less decelerating in this region. Thus, after having been pushed forward by the main pulse ponderomotive force, the electrons in this region are less decelerated and can then enter the

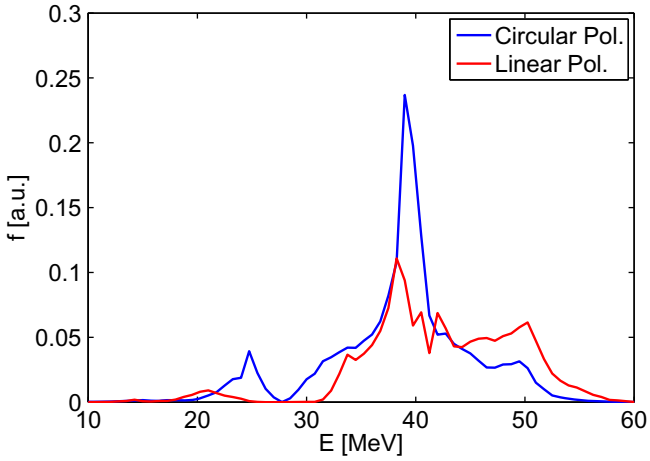

Figure 10. Electron distribution after an acceleration over 0.6 mm in the linear and circular polarizations cases. The counter-propagating pulse is characterized by $a_1 = 0.4$ and $\tau_1 = 45$ fs.

bubble with the necessary momentum to be injected. Therefore, wake inhibition can prevent the injection of the electrons dephased by the beatwave, as claimed in section 4, but it can also induce this additional injection. This injection occurs here because a more intense colliding pulse is used, which enhances the wake inhibition. However, it did not occur in simulations previously presented, because wake inhibition was lower and only cold injection could occur.

The comparison of the two simulations clearly shows that warm injection leads to the injection of a bunch with a larger volume in phase space, which could lead to an increase in the beam energy spread. This situation is usually not desired. This consequence on the energy spread is confirmed by the electron distribution obtained after a short acceleration: as shown in figure 10, a quasi-monoenergetic peak is created with circular polarizations, whereas a wider peak is created with linear polarizations. In the circular polarization case, we have checked that the cold-injected electrons create this peak. In the linear polarization case, part of the electrons that were cold injected in the simulation with circular polarizations are strongly accelerated by the stochastic heating. Therefore, these electrons are spread in phase space by the heating. This phenomenon increases the energy spread and reduces the amplitude of the quasi-monoenergetic peak, as observed in the distribution shown in figure 10.

Therefore, as shown in the first example, if cold injection is not possible, relying on warm injection would obviously be required. In contrast, as shown in the second example, when a low plasma density and an injection pulse with a low intensity are used, warm injection does not occur and cold injection is the sole mechanism leading to injection. Between these two cases, if cold and warm injections can occur together, using circular polarizations to avoid warm injection might be preferable. In addition, using a colliding pulse with a short enough duration and a low enough intensity might be useful to avoid an additional injection due to wake inhibition. If this additional injection does not occur and if the colliding parameters are carefully chosen, a bunch of electrons can be dephased and injected while keeping a low-energy spread.

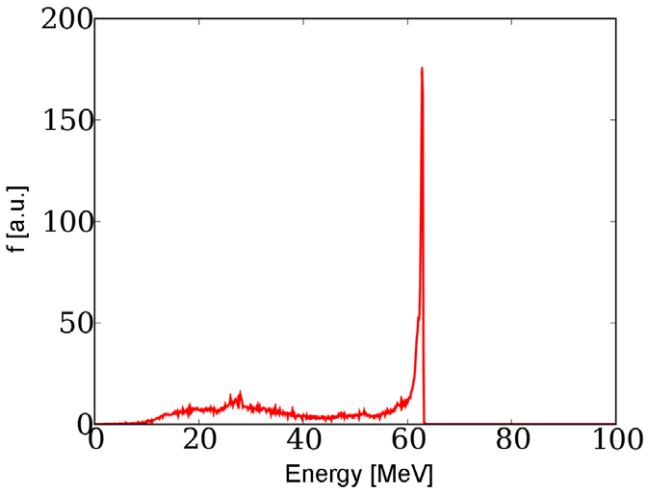

Figure 11. Electron distribution obtained after an acceleration over 0.6 mm with a constant plasma density in the transverse direction (2D simulation).

7. Production of multi-GeV bunches with narrow energy spread

In this section, we present the results of simulations where we have modeled both the injection and acceleration of electrons. As optical injection allows us to inject electrons in a wake created at low plasma density, the electrons can be accelerated over a long distance before reaching the dephasing length. Thus, as shown in the following where a multi-GeV beam is produced with 4 J of laser energy, high-energy electron beams can be obtained. Thanks to the cold injection scheme, these beams can be produced with narrow energy spread.

In the simulations presented below, the main and counter-propagating laser pulse parameters are $a_0 = 4$, $\Phi_0 = 18\,\mu$m, $\tau_0 = 30$ fs and $a_1 = 0.1$, $\Phi_1 = 15\,\mu$m, $\tau_1 = 30$ fs.

In a first 2D simulation, in which the plasma density is constant at $n_e = 2.5 \times 10^{-4} n_c$, a 62 MeV beam is produced after acceleration over 0.6 mm. The corresponding electron distribution is given in figure 11. The cold injection mechanism allows us to obtain a monoenergetic peak with a low absolute rms energy spread $\Delta E = 0.7$ MeV (calculated for electrons above 60 MeV), corresponding to a relative spread $\Delta E/E = 1.1\%$. The 2D beam charge (above 60 MeV) is 3 pC μm^{-1}, which approximately corresponds to a 50 pC beam if we assume that the transverse characteristic length is of the order of the pulse waist (18 μm). Therefore, these results confirm that a beam with very narrow absolute energy spread can be produced by the cold injection scheme.

In a second simulation, as described in section 3, a parabolic plasma profile is used to guide the main pulse. In that case, a 3.8 pC μm^{-1} bunch is injected. When it reaches 60 MeV, its energy spread is larger than in the previous simulation, as an energy spread of 10% is measured. This bunch reaches the dephasing length after an acceleration over 3.8 cm. After this acceleration, a 3 GeV beam is obtained, with the energy spectrum shown in figure 12. The energy spread of electrons over 2.9 GeV is 0.9%.

The final energy spread depends on two parameters: (i) the initial energy spread and (ii) the evolution of the energy spread during the acceleration. As shown in figure 11, the cold injection mechanism can be an interesting option to inject a beam with a low initial energy

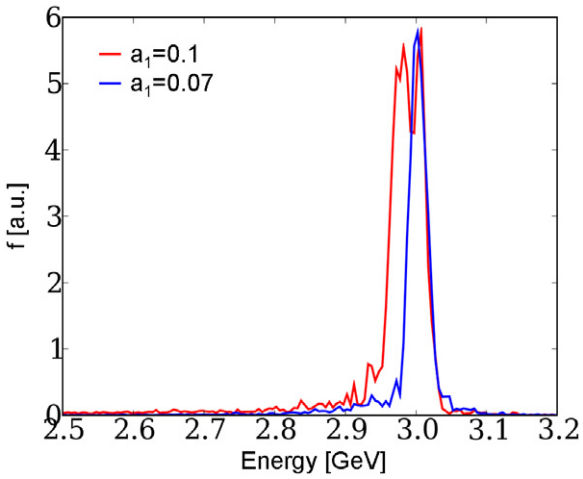

Figure 12. Electron distributions obtained after acceleration over 3.8 cm with a parabolic plasma density in the transverse direction (2D simulation).

spread. The evolution of the energy spread is determined by the beam-loading effects [33, 34]. If the beam current optimizes the beam-loading effects, then the absolute energy spread remains constant during the acceleration, so the relative energy spread decreases with energy gain. If the beam current is not at the optimal value, then the absolute energy spread increases during acceleration.

In the last simulation, the beam-loading effects are not optimized. Therefore, the energy spread can still be improved by injecting a lower charge. By using a counter-propagating pulse with lower intensity, with $a_1 = 0.07$, a 1.8 pC μm^{-1} electron beam is injected, and an energy spread of 0.45% is obtained when the bunch reaches 3 GeV. The rms beam duration is then 4.8 fs and the rms transverse emittance is 8.1 mm mrad (with rms transverse emittance defined as $\epsilon_y = 1/(m_e c)[\langle y^2\rangle\langle p_y^2\rangle - \langle y p_y\rangle^2]^{1/2}$ where y and p_y are the transverse position and momentum).

A 3D simulation is needed to calculate a real beam charge and to validate the 2D results that show that a multi-GeV beam with narrow energy spread can be obtained. However, to simulate acceleration over a few cm in a 3D geometry requires too much computing resources with a conventional PIC code. We have then used the Calder–Circ reduced PIC code, described and benchmarked in [35], which, by assuming quasi-radial symmetry, allows us to model wakefield acceleration with similar results to a full 3D simulation, but with a speedup of two orders of magnitude.

Calder-Circ has been used to simulate the case with $a_1 = 0.1$. The simulation shows that a 59 pC bunch is injected, which is close to the extrapolated 2D result. This bunch reaches the dephasing length after acceleration over 3.3 cm and is accelerated up to 2.7 GeV at that point, as shown in figure 13. The final energy spread is 2.2%. Reducing this energy spread may also be possible by tuning the value of a_1, as shown with the 2D simulations. These results confirm the 2D conclusion: thanks to the cold injection scheme, a multi-GeV beam with energy spread in the range of 1% and with a charge of several tens of pC can be generated with a 4 J laser pulse.

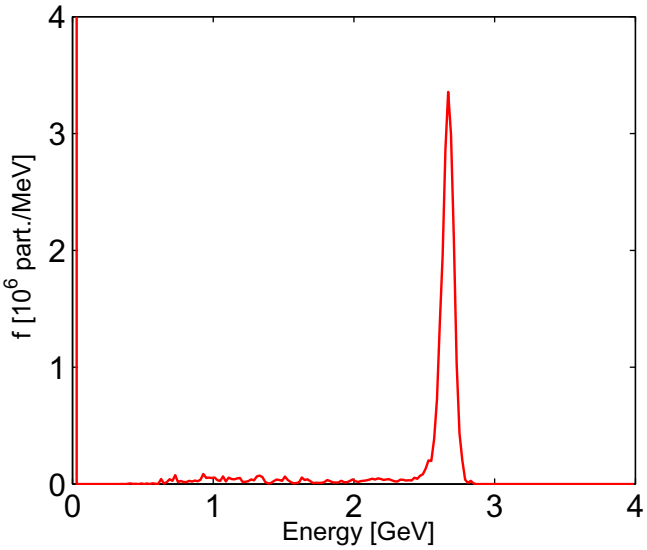

Figure 13. Electron distribution obtained with the quasi-radial PIC code Calder-Circ [35].

8. Conclusions and discussion

In this paper, we have given an analysis of the cold injection scheme, which was first presented in [23]. In this scheme, the electrons are first dephased without heating by the beatwave, before being injected. First, a 1D simplistic model determining which electron is dephased was presented and compared with simulations in the paper. Then, some conditions for the existence of this scheme were determined. We have also shown that off-axis electrons can be injected, thanks to this scheme, and due to transverse effects they can even be injected more easily than on-axis electrons. Comparison with a previous injection scheme based on heating is carried out. We have shown that these two mechanisms, cold and warm injections, can occur for different ranges of plasma and laser parameters. However, when the two mechanisms can exist together, relying only on the cold injection can be preferable to inject a bunch with a lower energy spread. Eventually, thanks to simulations including both injection and acceleration, we have shown that this scheme is able to inject electron bunches with narrow initial energy spreads in the wake. Our simulations also show that a multi-GeV electron beam with a final energy spread of the order of 1% can be obtained.

The results presented in this paper provide a better understanding of the advantages and limits of the cold injection scheme. They also open the way for deeper analyses. For instance, modifying the counter-propagating laser pulse parameters should lead to the possibility to tune the electron beam parameters and improve its quality.

This issue of beam quality is relevant for several applications. For example, producing high-energy beams with extremely good quality is important for coherent x-ray generation, like in the X-FEL concept, in which the beam wiggles in an undulator. We thus conclude our paper by discussing the potential of the beams that we have calculated in our simulations for FEL. To create an FEL, the relative energy spread of the beam should be smaller than the so-called Pierce parameter ρ defined in [36]. The Pierce parameter depends on the undulator characteristics and is also proportional to $\gamma^{-1} I^{1/3} \sigma_x^{-2/3}$, where γ is the Lorentz factor of the

electrons, I the beam current and σ_x the transverse size of the beam. σ_x is mainly determined by the beam emittance and the focusing system of the undulator. The beam emittance of a few mm mrad calculated in section 7 is of the same order of magnitude as the emittance obtained in the typical conventional accelerators used for x-FEL [37]. So, if the same undulator is used, then the value of σ_x might be in the same range in both the cases. The beam current obtained in our simulations, which is close to 10 kA, is also at the same level as the best values obtained in conventional accelerators. However, for typical x-FEL [37], multi GeV beams are required to produce x-rays, and the Pierce parameter is then typically in the range of $\rho \sim 10^{-3}$–10^{-4}. Electron beams with extremely narrow relative energy spread are then needed, which still seems far from what wakefield accelerators are able to produce at present. This can be improved by better control of the injection in order to accelerate a beam with a low initial absolute energy spread, as presented in this paper, and by controlling the beam-loading effects. A different solution consists in relying on beams with a few hundreds of MeV to increase the Pierce parameters to $\rho \sim 10^{-2}$. This value is more compatible with the relative energy spread found in our simulation, but the radiation wavelength, which scales as γ^{-2}, will increase and will no longer be in the x-ray energy range. Finally, it might also be possible to produce x-rays with a sub-GeV beam using new FEL concepts, as, for example, proposed in [38].

Acknowledgments

This work was performed using HPC resources from GENCI-CCRT (grants 2009-t2009056062 and 2010-x2010056304). VM acknowledges support from the European Research Council through the PARIS ERC project (contract number 226424). AB was partially supported by LASERLAB-EUROPE/LAPTECH, EC FP7 contract number 228334.

References

[1] Tajima T and Dawson J M 1979 Laser electron accelerator *Phys. Rev. Lett.* **43** 267
[2] Mangles S P D *et al* 2004 Monoenergetic beams of relativistic electrons from intense laser–plasma interactions *Nature* **431** 535–8
[3] Geddes C G R, Tóth Cs, van Tilborg J, Esarey E, Schroeder C B, Bruhwiler D, Nieter C, Cary J and Leemans W P 2004 High quality electron beams from a laser wakefield accelerator using plasma-channel guiding *Nature* **431** 538–41
[4] Faure J, Glinec Y, Pukhov A, Kiselev S, Gordienko S, Lefebvre E, Rousseau J-P, Burgy F and Malka V 2004 A laser–plasma accelerator producing monoenergetic electron beams *Nature* **431** 541–4
[5] Leemans W P *et al* 2006 GeV electron beams from a centimetre-scale accelerator *Nat. Phys.* **2** 696–9
[6] Hafz N *et al* 2008 Stable generation of GeV-class electron beams from self-guided laser–plasma channels *Nat. Photon.* **2** 571–7
[7] Butler A, Spence D J and Hooker S M 2002 Guiding of high-intensity laser pulses with a hydrogen-filled capillary discharge waveguide *Phys. Rev. Lett.* **89** 185003
[8] Faure J, Rechatin C, Norlin A, Lifschitz A, Glinec Y and Malka V 2006 Controlled injection and acceleration of electrons in plasma wakefields by colliding laser pulses *Nature* **444** 737–9
[9] Faure J Ź, Rechatin C Ő, Lifschitz A F, Davoine X, Lefebvre E and Malka V 2008 Experiments and simulations of the colliding pulse injection of electrons in plasma wakefields *IEEE Trans. Plasma Sci.* **36** 1751–9
[10] Faure J, Rechatin C, Ben-Ismail A, Lim J, Davoine X, Lefebvre E and Malka V 2009 Physics of colliding laser pulses in underdense plasmas *C R Phys.* **10** 148–58

[11] Malka V, Faure J, Rechatin C, Ben-Ismail A, Lim J K, Davoine X and Lefebvre E 2009 Laser-driven accelerators by colliding pulses injection: a review of simulation and experimental results *Phys. Plasmas* **16** 056703
[12] Rechatin C, Faure J, Ben-Ismail A, Lim J, Fitour R, Specka A, Videau H, Tafzi A, Burgy F and Malka V 2009 Controlling the phase-space volume of injected electrons in a laser–plasma accelerator *Phys. Rev. Lett.* **102** 164801
[13] Malka V, Faure J, Gauduel Y A, Lefebvre E, Rousse A and Phuoc K Ta 2008 Principles and applications of compact laser–plasma accelerators *Nat. Phys.* **44** 447–53
[14] Grüner F *et al* 2007 Design considerations for table-top, laser-based VUV and X-ray free electron lasers *Appl. Phys.* B **86** 431–5
[15] Bulanov S, Naumova N, Pegoraro F and Sakai J 1998 Particle injection into the wave acceleration phase due to nonlinear wake wave breaking *Phys. Rev.* E **58** R5257–60
[16] McGuffey C *et al* 2010 Ionization induced trapping in a laser wakefield accelerator *Phys. Rev. Lett.* **104** 025004
[17] Pak A, Marsh K A, Martins S F, Lu W, Mori W B and Joshi C 2010 Injection and trapping of tunnel-ionized electrons into laser-produced wakes *Phys. Rev. Lett.* **104** 025003
[18] Umstadter D, Chen S-Y, Maksimchuk A, Mourou G and Wagner R 1996 Nonlinear optics in plasmas and laser wake field acceleration of electrons *Science* **273** 472
[19] Hemker R G, Tzeng K-C, Mori W B, Clayton C E and Katsouleas T 1998 Computer simulations of cathodeless, high-brightness electron-beam production by multiple laser beams in plasmas *Phys. Rev.* E **57** 5920–8
[20] Esarey E, Sprangle P, Krall J and Ting A 1997 Self-focusing and guiding of short laser pulses in ionizing gases and plasmas *IEEE J. Quantum Electron.* **33** 1879–914
[21] Fubiani G, Esarey E, Schroeder C B and Leemans W P 2004 Beatwave injection of electrons into plasma waves using two interfering laser pulses *Phys. Rev.* E **70** 016402
[22] Kotaki H, Masuda S, Kando M, Koga J K and Nakajima K 2004 Head-on injection of a high quality electron beam by the interaction of two laser pulses *Phys. Plasmas* **11** 3296
[23] Davoine X, Lefebvre E, Rechatin C, Faure J and Malka V 2009 Cold optical injection producing monoenergetic, multi-GeV electron bunches *Phys. Rev. Lett.* **102** 065001
[24] Mora P and Antonsen T M Jr 1997 Kinetic modeling of intense, short laser pulses propagating in tenuous plasmas *Phys. Plasmas* **4** 217–29
[25] Davoine X, Lefebvre E, Faure J, Rechatin C, Lifschitz A and Malka V 2008 Simulation of quasimonoenergetic electron beams produced by colliding pulse wakefield acceleration *Phys. Plasmas* **15** 113102
[26] Lefebvre E *et al* 2003 Electron and photon production from relativistic laser–plasma interactions *Nucl. Fusion* **43** 629–33
[27] Mendonça J T 1983 Threshold for electron heating by two electromagnetic waves *Phys. Rev.* A **28** 3592–8
[28] Sheng Z-M, Mima K, Sentoku Y, Jovanović M S, Taguchi T, Zhang J and Meyer ter Vehn J 2002 Stochastic heating and acceleration of electrons in colliding laser fields in plasma *Phys. Rev. Lett.* **88** 055004
[29] Bourdier A, Patin D and Lefebvre E 2005 Stochastic heating in ultra high intensity laser–plasma interaction *Physica* D **206** 1–31
[30] Rechatin C, Faure J, Lifschitz A, Malka V and Lefebvre E 2007 Plasma wake inhibition at the collision of two laser pulses in an underdense plasma *Phys. Plasmas* **14** 060702
[31] Lu W, Huang C, Zhou M, Mori W B and Katsouleas T 2006 Nonlinear theory for relativistic plasma wakefields in the blowout regime *Phys. Rev. Lett.* **96** 165002
[32] Kalmykov S Y *et al* 2010 Numerical modelling of a 10-cm-long multi-GeV laser wakefield accelerator driven by a self-guided petawatt pulse *New J. Phys.* **12** 045019
[33] Tzoufras M, Lu W, Tsung F S, Huang C, Mori W B, Katsouleas T, Vieira J, Fonseca R A and Silva L O 2008 Beam loading in the nonlinear regime of plasma-based acceleration *Phys. Rev. Lett.* **101** 145002

[34] Tzoufras M, Lu W, Tsung F S, Huang C, Mori W B, Katsouleas T, Vieira J, Fonseca R A and Silva L O 2009 Beam loading by electrons in nonlinear plasma wakes *Phys. Plasmas* **16** 056705
[35] Lifschitz A F, Davoine X, Lefebvre E, Faure J, Rechatin C and Malka V 2009 Particle-in-cell modelling of laser–plasma interaction using Fourier decomposition *J. Comput. Phys.* **228** 1803–14
[36] Bonifacio R, Pellegrini C and Narducci L M 1984 Collective instabilities and high-gain regime in a free electron laser *Opt. Commun.* **50** 373–8
[37] Huang Z and Kim K-J 2007 Review of x-ray free-electron laser theory *Phys. Rev. STAB* **10** 034801
[38] Balcou P 2010 Proposal for a Raman x-ray free electron laser *Eur. Phys. J.* D **59** 525–37